Applied Thermal Engineering 183 (2021) 116182

Contents lists available at ScienceDirect

Applied Thermal Engineering

journal homepage: www.elsevier.com/locate/apthermeng

Comparison of electro-thermal performance of advanced cooling techniques for electric vehicle motors

Amitav Tikadar [1], David Johnston [1], Nitish Kumar, Yogendra Joshi, Satish Kumar [*]

The G.W. Woodruff School of Mechanical Engineering, Georgia Institute of Technology, Atlanta, GA 30332, USA

ARTICLE INFO

Keywords:
Permanent magnet synchronous motor (PMSM)
Jacket cooling
Cooling channel
Direct winding heat exchanger (DWHX)
Winding loss
Efficiency

ABSTRACT

Permanent magnet synchronous motors are commonly used in the powertrain of electric vehicles because of their high power and torque densities. Attempts to increase power and torque densities beyond the state-of-the-art often suffer from thermal limitations of the adopted winding-wire insulation class. In this paper, overall effectiveness of four different cooling technologies, namely conventional stator jacket cooling, embedded circular and rectangular cooling channel within stator core, and direct winding heat exchanger have been studied numerically. By realizing temperature dependent magnetic and material properties, winding and core losses, a two-way coupling algorithm has been utilized to study the detailed electro-magnetic and thermal performance of BMW i3 motor with aforementioned cooling techniques. The numerical results illustrate that the direct winding heat exchanger approach provides better electro-thermal performance in comparison to the other cooling techniques analyzed. On the contrary, embedded rectangular and circular channel in stator core adversely affect the electromagnetic performance and overall efficiency of the motor, despite their superior thermal performance compared to the jacket cooling.

1. Introduction

Electric motors play an integral role in the electrification of commercial electric vehicles. Automotive companies such as Tesla, Nissan, BMW, Toyota, Ford, General Motors, etc. which own a significant share of the all-electric and hybrid-electric vehicle markets, are striving to make high torque and high power density motors [1]. Heat removal is currently a limiting factor in achieving higher torque ratings for electric motors, with some heat generation in the literature ranging between few hundred watts to few kilowatts depending on the motor type, speed, and loading [2-4]. Without appropriate thermal management, high temperatures could damage insulation in the copper windings [5]. Namely, the thermal limits for Class F and Class H insulation are listed as 155 °C and 180 °C, respectively, but components can fail at temperatures as low as 60 °C [6,7]. For permanent magnet motors, high temperatures can also initiate demagnetization of magnets embedded in the rotors [7]. In response to these engineering problems, several thermal management techniques have been proposed in the last decade.

Electric motors are primarily cooled by air, but liquid cooling is becoming common nowadays to achieve higher power density. Air-cooling is the least expensive thermal management technique, and to date, various studies have been performed to optimize the performance of air-cooled designs. Kim et al. [8] positioned two microscopic fans each with 18 airfoil-shaped wings on the rotary shaft at both ends of the stator-rotor air gap of an induction motor. The authors studied the electromagnetic and thermal responses of the motor using a coupled model developed in ANSYS Maxwell/FLUENT, which showed that the aforementioned fan arrangement improved heat transfer. In another study, Zhang et al. [9] developed an experimentally validated coupled model to predict the electromagnetic losses and temperatures for an air-cooled induction machine. Coupled modeling frameworks improve the accuracy of the model, because the copper losses in the windings are largely dependent on temperature and vice versa. In general, air-cooled methods require less maintenance than other cooling techniques, but have a disadvantage of lower heat dissipation capability [7].

Liquid cooling is needed to maintain temperature in windings below the threshold in high power density motors. Superior thermo-physical properties of liquid coolants lead to higher heat transfer coefficients and consequently, lower motor temperature. One of the commonly used liquid cooling configuration for motors is a peripheral water jacket, typically attached to the outer surface of the stator inside a motor

* Corresponding author.
E-mail address: satish.kumar@me.gatech.edu (S. Kumar).
[1] These authors contributed equally to this work.

https://doi.org/10.1016/j.applthermaleng.2020.116182
Received 4 July 2020; Received in revised form 3 October 2020; Accepted 5 October 2020
Available online 12 October 2020

Nomenclature

Tr	torque, N.m
m	number of phase
p	pole pair
I	current,A
L	inductance,mH
S	skewness factor
n	harmonic order
N	maximum harmonic order
B	magnetic flux density,T
P	power,W
f	frequency,Hz
r	radius,m
R	resistivity,$\Omega.m$
a	coefficient of resistivity,$1/K$
T	temperature,K
k	thermal conductivity,$W/m.K$
D	diameter,m
q'''	heat generation, W/m^3
h	convection coefficient,$W/m^2.K$
v	fill factor

Greek symbols

λ	magnetic flux linkage, Wb
δ	rotor angle, EDeg
φ	phase angle, Edeg
α	temperature coefficient,%/$^\circ$C
ω	shaft speed,rad/s
θ	angular
η	efficiency

Subscripts

e	electro-magnetic
d	direct
q	quadrature
mag	magnet
$skew$	skewness
ms	magnetic skewness
res	residual
s	shaft
a	ambient
w	winding
out	output
r	radial
z	axial
sur	surface
f	fluid
c	copper
im	impregnation

housing. Multiple studies for the analysis of water jacket's performance have been reported. Satrustegui et al. [10] developed a coupled electromagnetic-thermal model using Cedrat Flux 3D for spiral, axial, and U-shaped duct arrangements in a water-jacket. Through both numerical and experimental analysis, the authors demonstrated that higher heat transfer coefficients can be achieved by adding vanes to the water jacket. Pyrhonen et al. [3] also performed a coupled electromagnetic-thermal analysis of motor using Cedrat Flux 3D. They implemented high conductivity copper bars to bridge heat transfer path between the stator core and the water jacket. Lundmark and Acquaviva [11] performed a coupled numerical analysis on a water jacket cooled internal permanent magnet motor using ANSYS Maxwell and FLUENT. Their analysis showed that the transverse flux motor demonstrated fewer hot spots than a radial flux motor.

In contrast to jacket cooling, which is employed externally to the stator, cooling channels can be employed in the stator and rotor cores. This cooling technique has been adopted by multiple industries. For example, Rolls Royce implemented circular channels to the stator core of a PMSM motor [12], while Siemens AG also designed stator cooling channels adjacent to the windings for high power generators [13]. Similarly, rectangular channels were implemented in the stator core for cooling of the Tesla Model 3 [14]. Kumar et al. [15] performed finite element analysis of various cooling channel geometries to determine how the electro-magnetic response depends on their shape and to optimize their design. In order to enhance motor specific power rating, Lee et al. [16] proposed a unique rotor cooling technique utilizing a hollow shaft, along with conventional housing cooling. A special coolant flow path facilitated coolant circulation from the stator housing to the rotor via the hollow shaft. The authors performed coupled electro-thermal analysis and experiments to demonstrate superior electro-thermal performance of the proposed cooling method over air-cooling and jacket cooling methods.

Cooling techniques which implement phase change materials (PCM) and spray cooling have also appeared in recent literature. For example, Wang et. al injected a paraffin PCM into the casing of a PMSM and found that the latent heat driven cooling extended the operating time by 50% [17]. The authors developed a similar implementation of a PCM into a fin-cooled PMSM, which extended motor run time by 32.7% [18]. Park and Kim [4] studied channel cooling and spray cooling and found that the addition of spray cooling to the stator provided a moderate decrease in temperature compared to cooling channels alone, and these enhancements were greater at higher speeds. Similar spray cooling techniques has also been studied by many other researchers [19–22].

Semidey and Mayor [6] demonstrated direct winding heat exchanger (DWHX), which utilize individual cooling channels embedded in the windings within stator slots. Heat is rejected to the fluid in the channels located along the axial direction of the motor. This single phase cooling technique showed significant improvements by using micro-features in the heat exchanger channels, with heat transfer coefficients as high as 50,000 $W/m^2.K$ [23]. The effectiveness of DWHX has also been numerically and experimentally verified by many other researchers [24,25].

Although electro-magnetic and thermal performance of electric machines are strongly dependent on each other, many of the previous studies have not considered the effect of cooling strategy on electromagnetic performance. For example, Xiong et. al. [26] developed an algorithm to iteratively determine the efficiency of a three-level brushless synchronous generator and found that higher speeds and higher loading each led to increased efficiency. Silwal et al. [27] provided a detailed comparison of water jacket cooling, DWHX cooling, and combined water jacket and DWHX cooling based on the temperature distribution and mechanical stresses induced in the windings. However, the authors did not explore the dependence of electro-magnetic performance on the temperature distribution, or vice versa. Similarly, Semidey and Mayor [6] did not present electro-magnetic performance of DWHX incorporated motor, and did not directly compare the DWHX technique with other cooling techniques.

From the above literature survey, it can be seen that despite of strongly coupled electro-magnetic and thermal performance of electric machine, to date, very few coupled electro-thermal analysis have been performed, especially for enhanced cooling techniques. Additionally, to the best of the author's knowledge, to date, no detailed comparative

study of different stator and slot cooling strategies has been performed for BMW i3 motor. In this study, a detailed comparison of three different advanced cooling techniques namely direct stator cooling using rectangular and circular channel, and direct winding heat exchanger (DWHX) have been performed with the conventional jacket cooling technique. All above mentioned cooling techniques were incorporated in a 125 kW BMW i3 motor topology and a coupled electro-thermal solving algorithm has been utilized to compare the effect of different cooling techniques on the overall performance of the motor. Electromagnetic and thermal simulations were iteratively performed using finite element (FE) based electro-magnetic software Motor-CAD® and computational fluid dynamics (CFD) software ANSYS Fluent®, respectively. Outputs such as inductance, torque, winding and stator losses, and peak winding temperatures for each cooling technique were assessed under numerous electrical loading conditions to provide guidelines for the thermal management system selection and their subsequent effects on overall motor performances.

2. Machine topology and cooling methods

Interior permanent magnet synchronous motor (IPMSM) topology of a jacket cooled BMW i3 motor with a peak power and torque of 125 kW and 250 N.m, respectively [28], has been chosen as a base configuration. Fig. 1 illustrates the front and side views, and Table 1 summarizes detailed specifications of conventional BMW i3 motor. Two layers of Sintered Neodymium-Iron-Boron magnet, N42UH [29], and four flux barriers have been added per pole. Moreover, in order to reduce the cogging torque and torque ripple, the rotor and magnet are sliced into six axial segments and stacked in a skewed fashion [28]. An aluminum sheath is shrink-fitted onto the outer diameter of the stator, and the outer surface of the sheath has a spiral channel to form a circulating cooling path with the outer housing as shown in the Fig. 1(b).

In high torque density machines like BMW i3, major heat losses occur in the windings in the form of Joule heating. For a jacket cooled motor, dissipated heat from the windings needs to transfer to the coolant via slot liner, stator lamination, and finally stator frame (see Fig. 1). In addition to the thermal resistances of these components, contact resistances at winding-liner, liner-lamination, and lamination-frame interfaces result in additional rise in winding temperatures. Heat generated due to the stator core losses is also a significant component of the total loss, which need to flow through the lamination-frame contact resistance. Therefore, thermal performance of the electric machine can be significantly enhanced by moving coolant channels closer to the heat sources, i.e., winding. However, shifting cooling channels towards windings may adversely affect electro-magnetic performance of the machine.

Table 1
Geometric and winding specifications of the jacket cooled BMW i3 motor.

Parameters (unit)	Value
Number of phase	3
Number of slot/pole	72/12
Stator OD (mm)	240.9
Stator ID (mm)	179.6
Air gap (mm)	0.5
Slot depth (mm)	21.5
Slot opening (mm)	2.5
Tooth tip depth (mm)	0.5
Active length (mm)	130
End-winding length (mm)	32
Inner layer magnet thickness (mm)	6
Outer layer magnet thickness (mm)	3.2
Stator/rotor lamination	M250-35A
Winding configuration	
Number of turns per coil	9
Number of strands in hand	12
Parallel path	6
Wire OD (mm)	0.7
Wire ID (mm)	0.6
Total number of wire	108
Inter-wire distance	0.1
Copper slot fill factor	0.3332

Stator cooling channels can improve the thermal performance of the BMW i3 motor by directly extracting heat from the stator lamination. In this paper, two different stator cooling channels, namely circular and rectangular cross-section channels, have been considered as shown in the Fig. 2 (a) and (b). By integrating cooling channels in the stator lamination, conduction thermal resistance can be significantly reduced by shortening the distances between the winding slot and coolant, and also by eliminating the lamination-housing contact resistance. Another advantage of direct stator cooling is that it only requires a thin housing to protect the machine from ambient, compared to the relatively thick housing needed for jacket cooling. Therefore, high power and torque density can be achieved by reducing housing weight. Moreover, circular and rectangular cooling channels in the stator core can be fabricated with a minimal cost by cutting the circular and rectangular shapes in the laminated sheet and channel are created automatically after the stamping of the laminated sheet. Additionally, direct stator cooling channels are applicable for any winding configuration and easy to

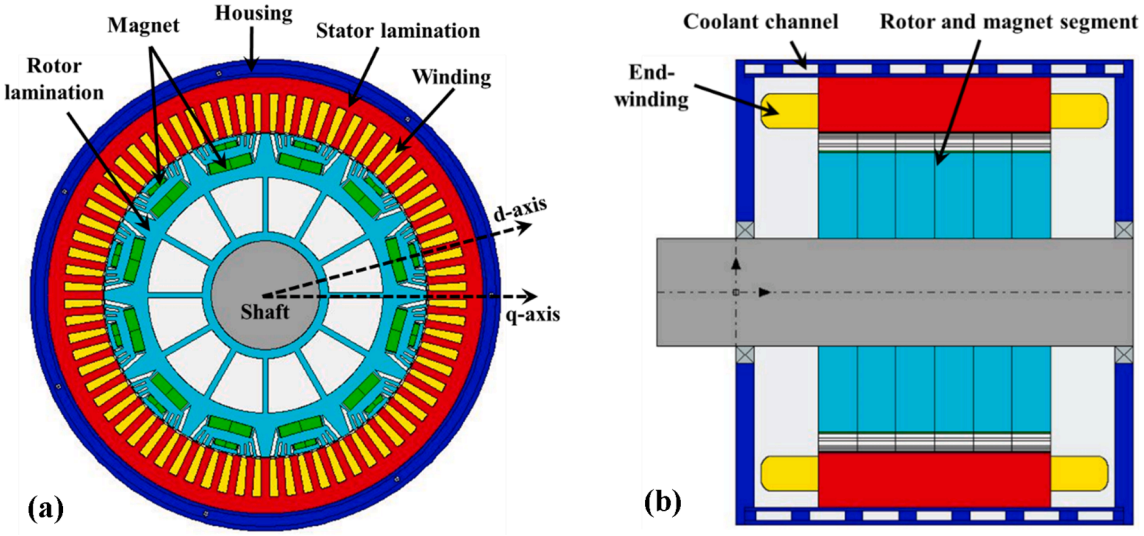

Fig. 1. (a) Front view and (b) side view of jacket cooled BMW i3 motor.

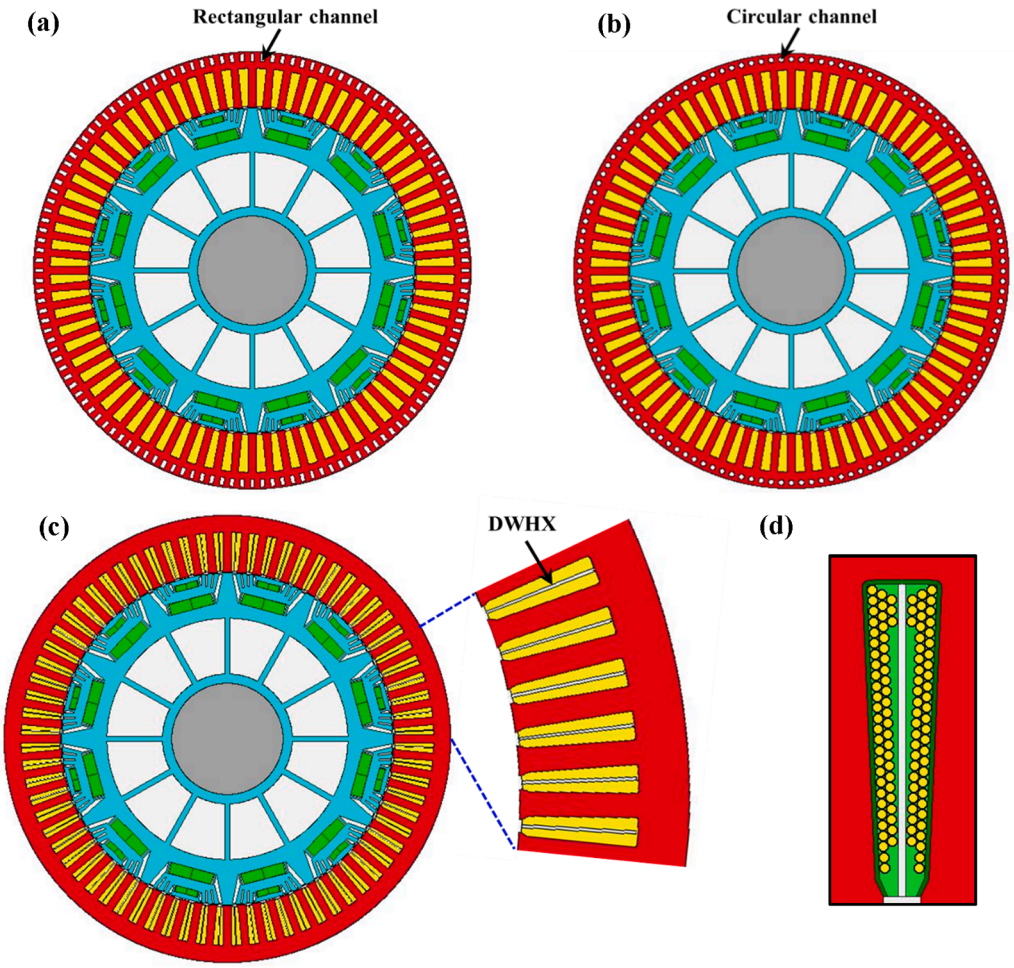

Fig. 2. Front view of (a) rectangular channel, (b) circular channel, (c) DWHX cooled motor, and (d) copper wires distribution in a DWHX cooled motor slot.

implement. However, direct stator cooling channels may saturate the stator core by adding extra magnetic flux resistance.

The rectangular channels in Fig. 2 (a) are 2.2 mm in width and 4.4 mm in height, having a hydraulic diameter of 2.93 mm. Each channel is placed at a 1 mm gap from the exterior periphery of the stator. The circular channels are sized at 2.93 mm diameter to maintain the same hydraulic diameter as the rectangular channels, and are centered in the same location as rectangular channels.

Windings to coolant thermal resistance can significantly reduce by employing DWHX in the stator slots as shown in the Fig. 2 (c). The DWHX transfers the winding heat directly into the coolant, resulting in significant reduction of the winding-coolant thermal resistance, which notably reduces the winding copper loss and hence, allows a substantial increase in current density without compromising with the winding thermal integrity. Additionally, eddy current induction and consequent eddy current loss in the DWHX can be prevented by utilizing non-conductive heat exchanger endcap/bulkhead [6]. Mass production of DWHX can be achieved either by utilizing 3D printing or can be fabricated into two parts and installed in the slot before impregnation/encapsulation [6 30]. However, a careful design is required to apply DWHX technology in a distributed wound machine. In case of DWHX, a 0.5 mm wide channel was placed into the center of each of the stator slot from top to bottom as shown in the Fig. 2 (d). The distance between copper wires in DWHX cooled windings has been reduced to 0.01 mm (see Fig. 2 (d)) to fit same number of the copper wire in each slot, while keeping all other parameters constant, which ensure same copper fill factor as jacket cooled and direct stator cooled machines.

3. Electro-magnetic simulation

3.1. Computational domain and governing equations

Figs. 1 and 2 illustrate fully assembled machine geometry, along with the corresponding cooling channels. Due to the symmetric distribution of the cooling channels and consequent magnetic flux, a single rotor pole and the corresponding stator configuration along with appropriate cooling channels has been considered as computation domain to reduce computational cost. In the case of a jacket cooled BMW i3 motor, aluminum (Al) housing is mounted on the stator lamination, and it is worth noting that the relative permeability of the Al housing (~1) is significantly lower than the stator lamination [31], resulting in entirely confined magnetic flux inside the stator core. Therefore, Al housing and spiral cooling channels (see Fig. 1) were not included in the electro-magnetic simulation domain.

Tr_e has been calculated using d and q-axis formulations (see Fig. 1 (a)) [32,33]:

$$Tr_e = \frac{m}{2}p\left(\lambda_d I_q - \lambda_q I_d\right) = \frac{m}{2}p\left[\lambda_{mag,d} I_q + \left\{I_d I_q \left(L_d - L_q\right)\right\}\right] \quad (1)$$

I_d and I_q have been calculated at each rotor position by applying the Park transformation [32].

For the skewed arrangement of the rotor lamination and magnets, the skewed flux linkage to the permanent magnet can be calculated by [33]:

$$\lambda_{mag,d} = \lambda_{skew}(\theta) = \sum_{n=1}^{N} S_{ms}\lambda_{mag} cos(n\delta + \varphi_n) \quad (2)$$

Where, S_{ms} is the magnet skewness factor [33,34].

Magnet flux linkage, λ_{mag} depends on the residual magnetic flux, B_{res} which has been calculated using the following equation [33]:

$$B_{res} = B_{res,ref(20)}\left(1 + \frac{\alpha\left(T_m - T_{ref.temp(20)}\right)}{100}\right) \quad (3)$$

Where, $B_{res,ref(20)} = 1.31T$ at reference temperature of 20 °C and the temperature coefficient (α) is −0.12%/°C [29].

Shaft torque (Tr_s) can be calculated as follows:

$$Tr_s = Tr_e - \left[\left(P_{core} + P_{mag}\right)/\omega\right] \quad (4)$$

Where, ω is the shaft speed, P_{core} and P_m are the core and magnet losses, respectively.

P_{core} has been calculated using modified Steinmetz iron loss model [33]:

$$P_{core}(W/kg) = K_h f.B^{\gamma+\vartheta B} + 2\pi^2 K_{eddy} f^2 B^2 \quad (5)$$

Where, K_h, γ, ϑ and K_{eddy} have been determined using curve fitting techniques in Motor-CAD. Since, electro-magnetic flux density depends on temperature, P_{core} depends on temperature.

P_{mag} has been calculated by knowing magnet eddy current from diffusion equation [33].

Copper/DC loss in the active and end-winding can be calculated by using the following equation [33]:

$$P_{DC} = 3I^2 R_a[1 + a_T(T_w - T_a)] \quad (6)$$

AC loss generated in the active section of winding has been calculated using the following equation [33]:

$$P_{AC} = \frac{\pi D^2(\omega B)^2}{128R_a[1 + a_T(T_w - T_a)]} \quad (7)$$

The overall efficiency of the machine can be calculated as follows:

$$\eta = \frac{P_{out}}{P_{out} + P_{DC} + P_{AC} + P_{core} + P_{mag}}$$

Where, $P_{out} = (Tr_s\omega)$ is the output power.

Moreover, mechanical and windage losses have been neglected in the electro-magnetic simulations. 2D finite element (FE) based software Motor-CAD has been used for the electro-magnetic simulations of motor for all integrated cooling techniques considered in the present work.

4. Heat transfer (HT) modeling

4.1. Computational domain and governing equations

Noting the axial and radial symmetry of the motor assembly, a 30° section in the radial plane and 1/6th section along the axial direction of the motor has been considered as the computational domain for HT modeling. Fig. 3 depicts the computational domains for all cooling techniques. The computational domain consists of one magnetic pole, six winding slots along with their corresponding liners, and the air gap between the stator and rotor, as shown in the Fig. 3.

The following assumptions have been made to simplify the HT analysis: (1) negligible radiation heat transfer, (2) end-windings effect on the motor thermal performance has been neglected, (3) steady state heat transfer, therefore thermal capacitances are negligible, (4) uniform distribution of heat sources in each region, (5) constant coolant temperature, and (6) isotropic thermal conductivity for all components, except winding, and stator and rotor laminations.

By considering the aforementioned assumptions, steady state 3D heat conduction equation in the cylindrical co-ordinate system [35] has been solved which can be written in the following form:

$$\frac{1}{r}\frac{\partial}{\partial r}\left(k_r r\frac{\partial T}{\partial r}\right) + \frac{1}{r^2}\frac{\partial}{\partial \theta}\left(k_\theta r\frac{\partial T}{\partial \theta}\right) + \frac{\partial}{\partial z}\left(k_z\frac{\partial T}{\partial z}\right) + q''' = 0 \quad (9)$$

Winding, stator, magnet, and rotor heat losses, calculated from electro-magnetic model, have been applied as volumetric heat sources in 3D HT model as shown in the Fig. 3 (a).

In order to reduce the computational cost to realize complex motor and cooling channel geometry and to assume fully developed flow conditions, liquid cooling has been simulated as a convection boundary condition on the coolant channel surfaces. For example, a constant heat transfer coefficient (h) is applied on the circular, rectangular, or DWHX channel's surfaces as shown in the Fig. 3 (b-d). For the case of jacket cooling, a constant h is applied on the stator outer surface (see Fig. 3 (a)). A similar approach for electric motor simulations has also been presented by previous studies [6,27,36].

$$-k\frac{\partial T}{\partial r} = h(T_{sur} - T_f) \quad (10)$$

Moreover, for all simulations, T_f has been considered as constant at 70 °C.

The heat transfer characteristics of the rotating rotor slot are complex. Available conventional convective heat transfer correlations of a stationary configuration are not valid for rotating rotor slot. Inside the rotating rotor slot, secondary air flow is generated, along with axial flow as a consequence of combined centrifugal and Coriolis effect, which can significantly change the heat transfer coefficient compared to the

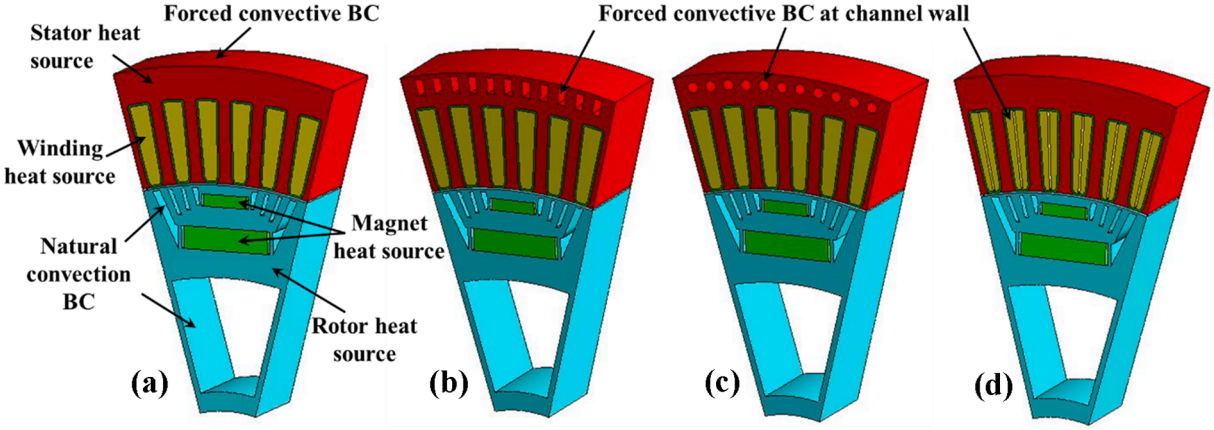

Fig. 3. Computational domain for thermal simulations (a) jacket cooling, (b) rectangular channel, (c) circular channel, and (d) DWHX.

stationary natural/forced convection [37]. To date, very few correlations for rotating smooth tube have been proposed considering rotating and axial Reynolds number [38]. All available correlations are strongly dependent on rotor slot and also entrance region configurations. Additionally, to the best of the author's knowledge, heat transfer correlations for BMW i3 motor rotor slot are not available in the open literature. Therefore, after realizing the complicated rotor duct geometry and to reduce the computational cost, a natural convective heat transfer coefficient of 10 $W/m^2.K$ has been chosen as a representative number for the numerical modeling and has been applied on all rotor slots (see Fig. 3 (a)).

Symmetric boundary condition is applied at the other boundaries, e.g. side, front, and back walls of stator, rotor, magnets.

Air flowing through the gap between the stator and rotor works as a convective heat transfer medium between the stator and rotor lamination. To avoid the modeling complexity of the coupled rotating air flow and convective heat transfer in the air gap, an effective static thermal conductivity of the air gap based on Reynolds number in the air gap has been utilized [39].

The geometry was meshed using the ANSYS meshing tool. In order to capture steep temperature gradient between the winding and the stator, very fine mesh was generated in the liner with a minimum resolution of 0.05 mm, as shown in the Fig. 4. Additionally, for individual configuration, appropriate mesh count has been selected via systematic mesh independence test. For example, in the case of DWHX, within a wide range of mesh resolution from 0.7 to 7.79 million, the peak winding temperature change was less than 0.02 °C. After realizing high computational cost for dense mesh, 1.4 million of mesh has been utilized for DWHX simulation. Similarly, 0.7, 0.74, and 0.66 1.4 million of mesh have been selected for jacket cooling, circular channel, and rectangular channel, respectively.

Finite volume (FV) based computational fluid dynamics and heat transfer (CFD/HT) software ANSYS Fluent® has been utilized for the HT simulations. Relative residual less than 10^{-12} has been set as convergence criteria for solution of the energy equations.

4.2. Effective thermal conductivity of the winding

Winding is a heterogeneous mixture of four different materials: copper wire, wire insulation, impregnation material, and air. However, the thermal properties of insulation materials i.e., wire insulation and impregnation materials are very similar. Therefore, it can be assumed that the winding only contains copper and impregnation and the Hashin and Shtrikman (H + K) approximation [40,41] has been used to estimate the effective radial/circumferential equivalent thermal conductivity of the winding:

$$k_{r/\theta} = k_{im}\frac{(1+v_c)k_c + (1-v_c)k_{im}}{(1-v_c)k_c + (1+v_c)k_{im}} \tag{11}$$

Where, k_c and k_{im} are the copper and impregnation thermal conductivity, v_c is the cooper fill factor.

On the contrary, axial equivalent thermal conductivity had been calculated from the parallel model for two materials. Effective orthotropic thermal conductivities of the winding have been calculated and summarized in Table 2. For the case of DWHX, reduced slot area and reduced distance between copper wires results in significantly higher effective conductivity in all directions as shown in the Table 2.

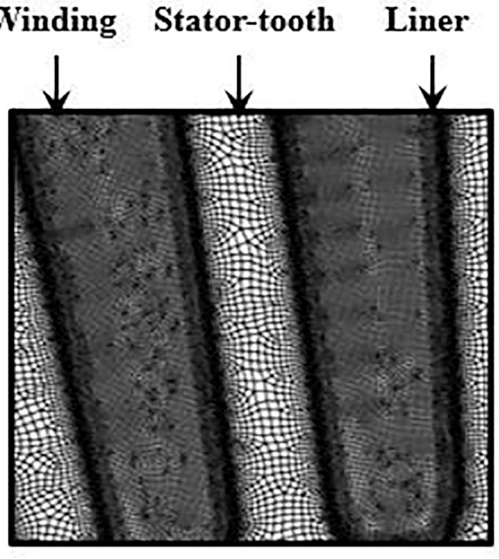

Fig. 4. Mesh generation for HT simulation.

5. Electro-magnetic and HT simulation coupling

From equations (1) to (8), it can be seen that B_{res}, λ_m, Tr_e, Tr_s, P_{DC}, P_{AC}, P_{core}, and η are strongly dependent on magnet and winding temperature and vice versa. Therefore, in order to accurately calculate the overall performance of the electric motor, electro-magnetic and thermal models need to solve in a coupled fashion. In this paper, a two-way coupling framework [42] has been utilized to perform electro-magnetic and HT simulations for all considered cooling configurations. In the first iteration, electro-magnetic simulation in Motor-CAD is performed using pre-assumed temperatures to calculate component wise heat losses in the motor components. Afterwards, the electro-magnetic losses are transferred as volumetric heat sources in the ANSYS Fluent® HT model, which simulates motor temperature distribution. After the first convergence of the HT model, motor component's temperature have been fed back into the electro-magnetic model to recalculate losses at the updated temperature. The above stated two-way coupled iterations are performed until the change in peak temperature of all individual components decreases below 0.5 °C. A detailed coupling algorithm can be found in our previous paper [42].

6. Numerical model validation

In order to validate the accuracy of the developed two-way coupled numerical model, shaft torque has been calculated under different electrical loading and compared with the benchmarking experimental results reported by Oak Ridge National Laboratory (ORNL) for a jacket cooled BMW i3 motor [28]. As shown in the Fig. 5, numerically calculated torque shows excellent agreement with the experimental data with an average deviation of less than 4.23%.

7. Results and discussion

7.1. Electro-magnetic Performance:

IPMSM produce high torque utilizing both alignment and reluctance torque. Alignment torque is generated by the interaction between the stator magneto-motive force (mmf) and d-axis (see Fig. 1 (a)) magnetic flux of buried-PMs in the rotor core. Reluctance torque generates from the saliency between d and q-axis (see Fig. 1 (a)). Since IPM machine torque greatly depends on L_d and L_q, respectively, understanding of flux flow path and any possible reluctances are necessary.

Table 2
Effect orthotropic thermal conductivity of the windings.

Cooling method	$k_r(W/m.K)$	$k_\theta(W/m.K)$	$k_z(W/m.K)$
Jacket and stator channel cooling	0.4609	0.4609	176.8
DWHX	0.7979	0.7979	246.6

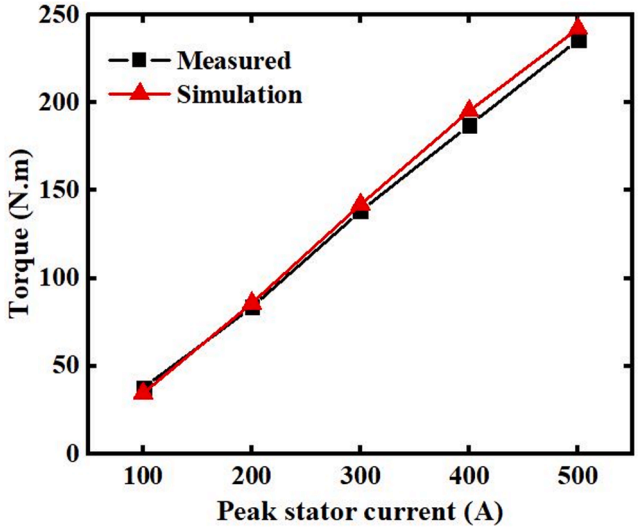

Fig. 5. Comparison between numerically calculated shaft torque and experimentally measured torque reported by ORNL [28] at 4500 rpm and heat transfer coefficient of 5,000 W/m^2.K.

Fig. 6 illustrates the magnetic flux density and flux line distribution under full load condition. Four layers of flux barriers along with top magnet layer, maximize stator and rotor flux interaction, i.e., flux density in the three stator tooth located in-between two rotor poles. From the figure, it can be seen that higher flux density generated in three inter-polar stator tooths, regardless of the stator cooling channel and DWHX. Moreover, cross-magnetization of armature reactions results in non-symmetrical flux distribution and torque ripple for all cases. For example, trailing corner of the rotor pole (left side) experiences highest magnetic flux density, in particular in the rotor bridge regions (see red circles in the Fig. 6). Additionally, the circular and rectangular stator channels block the flux flow path and reduce the permeance of the back iron region, which eventually results in back iron saturation under and top of the channels. Furthermore, higher perpendicular area of the rectangular channel to the flux flow path creates higher reluctance and consequently results in more flux saturation and leakage flux compared to the circular channel. Since DWHX is placed inside the slot, flux distribution for DWHX cooled machine is very similar as jacket cooling as depicted in the Fig. 6.

Fig. 7 shows the variation of d and q-axis inductances (L_d and L_q) as a function of the quadrature axis current (I_q) for each of cooling configurations. It can be seen that both L_d and L_q decrease as I_q increases because of the gradual saturation of the stator and rotor core. Additionally, two layers of magnet along d-axis work as flux barrier. This results in lower L_d and alignment torque compared to L_q and reluctance torque. Jacket cooled machine and DWHX cooled machine provide similar L_d and L_q regardless of I_q because of their alike flux distributions in the stator back iron region. On the contrary, for the circular and rectangular stator channels (see Fig. 2 (a) and (b)), L_d and L_q

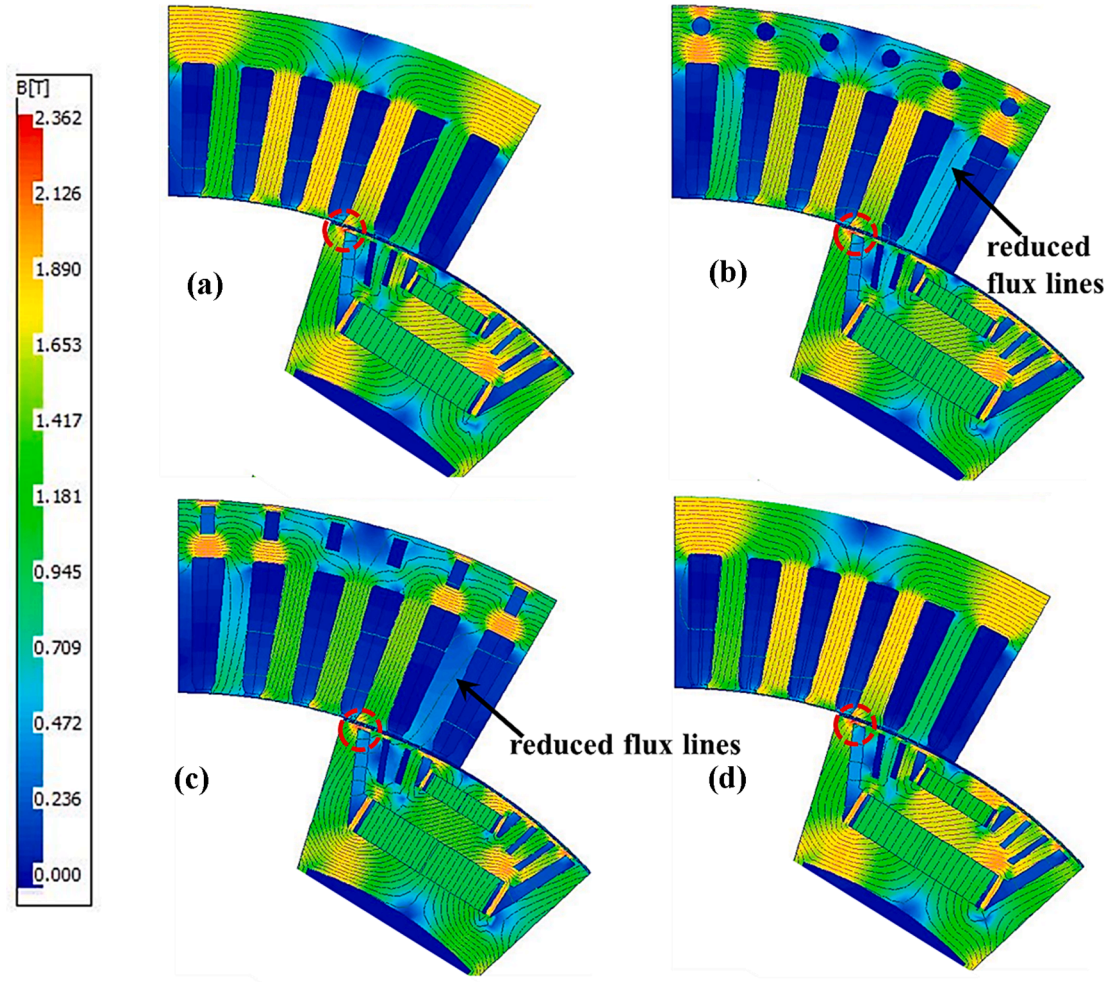

Fig. 6. Magnetic flux density distribution of (a) jacket cooling, (b) circular channel, (c) rectangular channel, and (d) DWHX while maintaining a constant speed, current density, phase advance, and convective heat transfer coefficient of 4,500 rpm, 17.37 A/mm^2, 45 EDeg, and 5,000 W/m^2.K respectively.

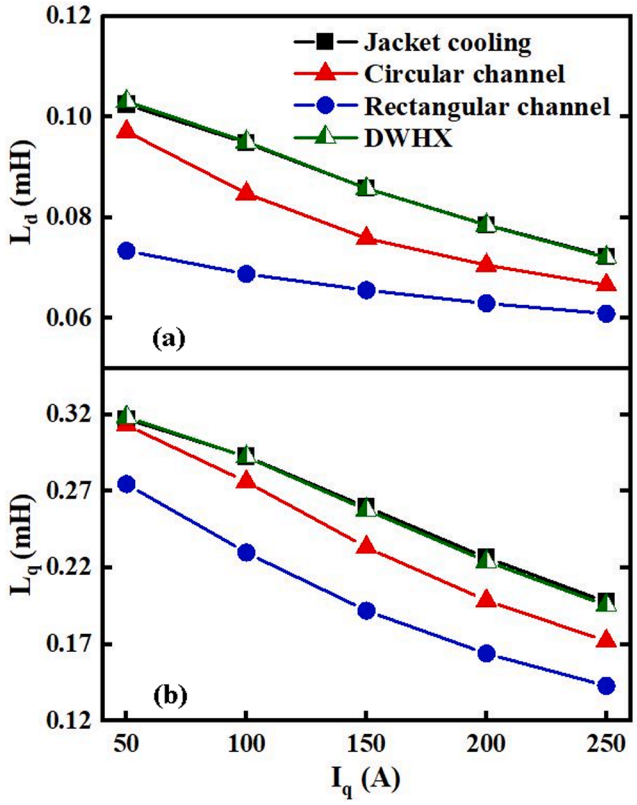

Fig. 7. (a) L_d vs I_q, and (b) L_q vs I_q at 4,500 rpm, 45 EDeg phase advance, and heat transfer coefficient of 5,000 W/m^2.K.

significantly reduce compared to the other two configurations. This behavior can be explained by recalling the inversely proportional relation between inductance and reluctance for same stator mmf. Since circular and rectangular channel increase reluctance by blocking the flux flow path in the stator back iron region (see Fig. 6), L_d and L_q decrease at any particular I_q, compared to the jacket and DWHX cooled machine. Moreover, higher reluctance of rectangular stator channel results in lower L_d and L_q compared to circular channel. For example, at 250A I_q for rectangular channel, L_d and L_q decrease by 15.74% and 27.82%, respectively compared to jacket cooled machine, whereas for circular channel, L_d and L_q decrease by 7.89% and 13%, respectively.

Higher stator reluctance for the same rotor configuration results in higher leakage flux and consequently lower air gap flux density (B_g). Fig. 8 illustrates B_g along the centerline of the air gap over a rotor pole (30 MDeg/180 EDeg) for all cooling configurations. From this figure, it can be observed that the circular and rectangular stator channels have lower B_g compared to other two cases because of the higher stator back iron reluctance and consequently reduced L_d and L_q as explained earlier.

Fig. 9 depicts the shaft torque as a function of rms current density for all cooling configurations. It can be observed that the PMSM modified with circular and rectangular stator channel provides significantly lower torque compared to the jacket cooled and DWHX cooled machines, especially at higher current densities. This can be attributed to the lower L_q and L_d (see Fig. 7), and consequently lower flux density, reluctance and alignment torque. For example, at a current density of 13.37A/mm^2 and for the case of circular and rectangular channels, shaft torque reduced by ~ 11.78 and 25.93%, respectively compared to the jacket cooling. On the contrary, at low current density, the circular stator channel provides lower L_d but similar L_q, and rectangular stator channel provides lower L_d and L_q compared to jacket cooled machine (see Fig. 7). However, the difference between L_d and L_q (~L_q-L_d) is comparable for all four cases and since reluctance torque is primarily determined by (L_q-L_d), circular and rectangular stator channels provide almost the same

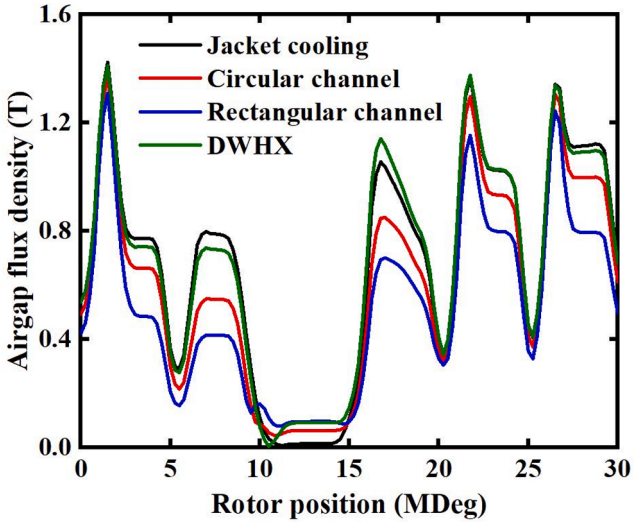

Fig. 8. Air gap flux density over a rotor pole for all cooling configurations at 4,500 rpm, 17.37 A/mm^2 current density, 45 EDeg phase advance, and heat transfer coefficient of 5,000 W/m^2.K.

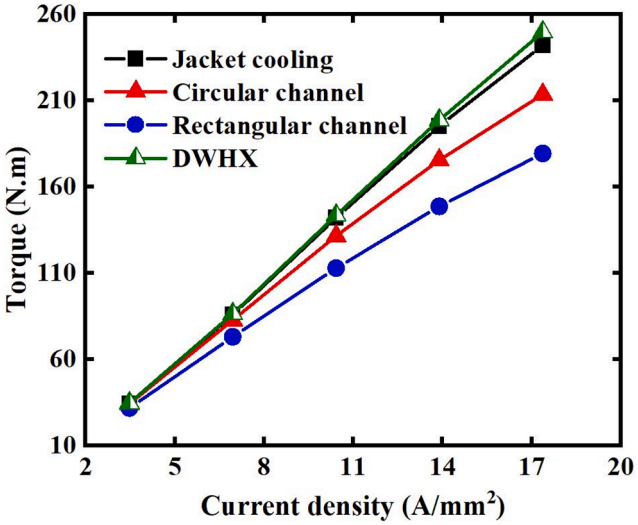

Fig. 9. Shaft torque vs. rms current density for all cooling configurations at 4,500 rpm, 45 EDeg phase advance, and heat transfer coefficient of 5,000 W/m^2.K.

shaft torque at the lowest current density of 3.47 A/mm^2 as shown in Fig. 9. Moreover, DWHX cooled PMSM provides mostly similar torque as jacket cooled machine, except at the highest considered electric load.

7.2. *Thermal Performance:*

Fig. 10 illustrates the temperature distributions for all considered cooling configurations. For the case of jacket cooling, maximum temperature occurs in the slot winding as shown in Fig. 10 (a). This can be attributed to the lower winding thermal conductivity and high conduction thermal resistance between the winding and the jacket. Similar temperature distribution is evident for the rectangular and circular channels (see Fig. 10 (b) and (c)). However, both direct stator cooling channels notably reduce the stator back iron conduction resistance, which eventually results in lower motor temperature compared to the jacket cooling as shown in the Fig. 10 (a)-(c).

It is also worth noting that the convective heat transfer area is 1366.1 *mm*^{2} for jacket cooling, 3146.0 *mm*^{2} for rectangular channel, and 2196.3

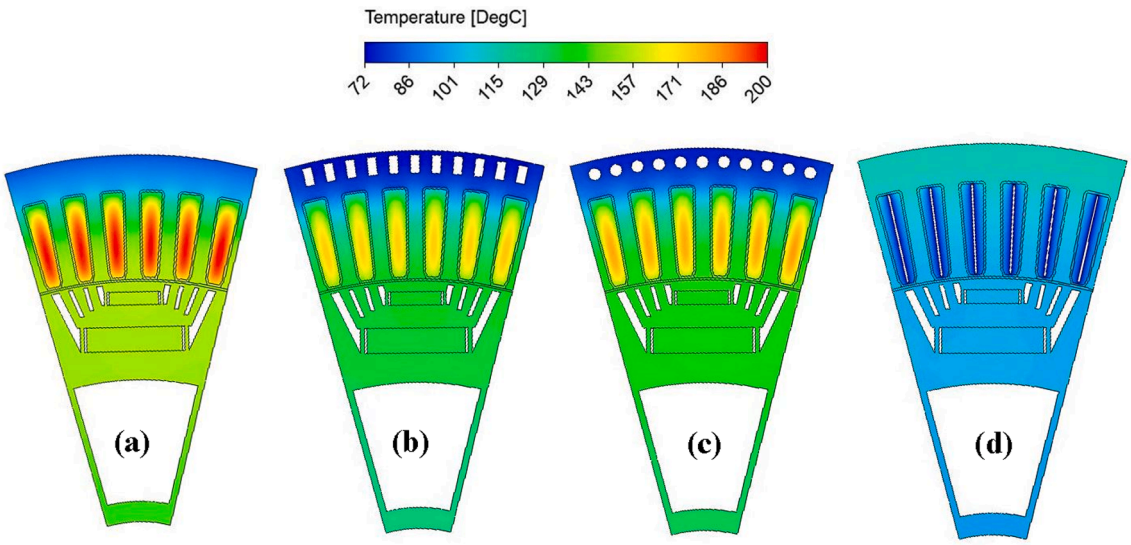

Fig. 10. Temperature distributions of (a) jacket cooled, (b) rectangular channel, (c) circular channel, and (d) DWHX cooled machine at 4,500 rpm, 17.37 A/mm^2 current density, 45 EDeg phase advance, and heat transfer coefficient of 5,000 W/m^2.K.

mm^2 for circular channel. Since in the case of rectangular and circular channel, convective heat transfer area increased by ~ 130% and ~ 61% compared to the jacket cooling, lower convective resistance attributes to reduce the motor temperature. Despite very similar conduction resistance, the rectangular channels were more effective in cooling than the circular channels (see Fig. 10 (b) and (c)) because of their higher convective surface area as explained earlier.

Among all cooling techniques considered, the DWHX is most efficient in reducing the peak temperature, as observed in Fig. 10 (d). Interestingly, the peak temperature is located toward the edge of the stator back iron rather than the windings, contrary to other cases. This can be attributed to the significantly higher convective surface area and reduced thermal resistance between winding and the coolant. The DWHX provides double the surface area compared to the circular channels and quadruple the surface area compared to the cooling jacket. Therefore, at the same heat transfer coefficient, the DWHX provides a much lower thermal resistance, which results in lower winding temperature.

Fig. 11 (a) illustrates the impact of convection heat transfer coefficients (h) on peak temperature for the four cooling techniques. Typical h for DWHX are between 500 and 1,000 W/m^2.K, and values as high as 50,000 W/m^2.K can be achieved using micro-structures and high flow rate of coolant [6]. Considering this window of h, a range of 1,000–11,000 W/m^2.K has been considered for simulations using DWHX. For all other cases, a range of 3,000–11,000 W/m^2.K has been considered for h. The results show that as h increased, the peak temperature reaches an asymptotic value. After increasing h beyond 10,000 W/m^2.K, only a marginal temperature decrease of ~ 1 °C is observed. DWHX and direct stator cooling techniques significantly reduce the motor temperature compared to the jacket cooling because of higher convective heat transfer area and reduced thermal resistance. For example, by employing DWHX, motor peak temperature can be reduced by ~ 88–102 °C compared to jacket cooling for h in the range of 3,000–11,000 W/m^2.K. The rectangular and circular channels also provide significant benefit over the jacket cooling by ~ 19–29 °C and ~14–20 °C, respectively.

Effects of all cooling techniques on the peak temperature under different electrical loading have been shown in Fig. 11 (b). DWHX, rectangular and circular channels provide significantly lower peak temperature compared to the jacket cooling, especially at higher current densities. For example, at current density of 17.37A/mm^2, peak temperature reduced by ~ 94 °C, 23 °C, and 17 °C by employing DWHX,

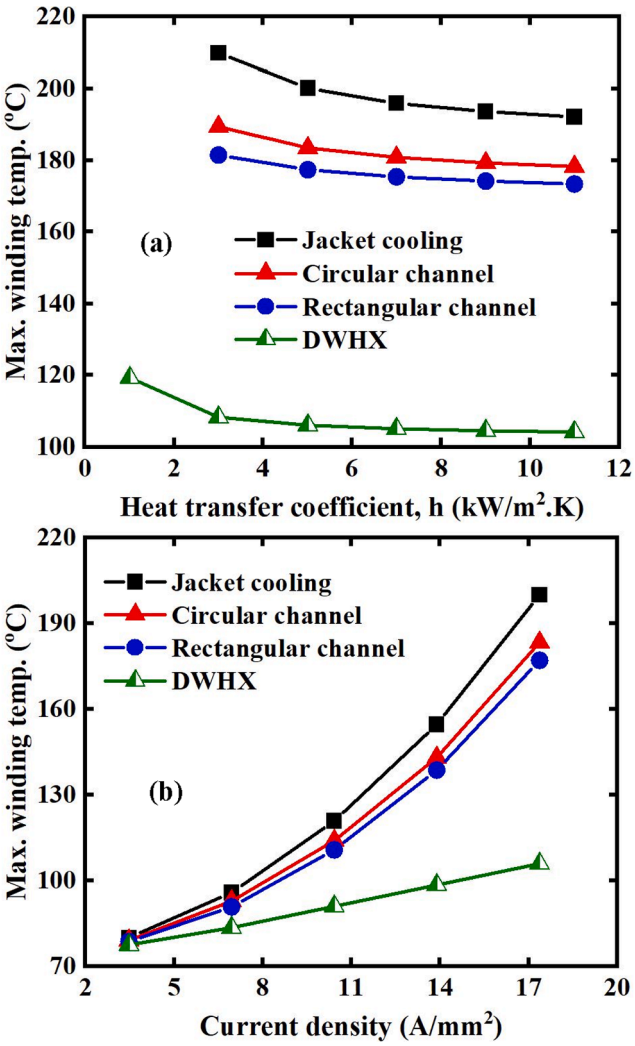

Fig. 11. (a) Peak temperature vs heat transfer coefficients at a current density of 17.37 A/mm^2, and b) peak temperature vs current density at heat transfer coefficient of 5,000 W/m^2.K. For all simulations, motor speed and phase advance were set at 4,500 rpm, and 45 EDeg.

rectangular, and circular channels, respectively.

7.3. Power Losses

Fig. 12 illustrates DC loss, AC loss, and total winding loss for all four cooling techniques under different electrical loading. DC loss occurs due to the resistive heating in the windings. Since DWHX cooling provides minimum temperature, followed by rectangular and circular channels as discussed earlier, winding resistances and consequently resistive losses follow the same trend, especially at higher current densities. For example, at a current density of 17.37 A/mm^2 and in cases of DWHX, circular and rectangular channels, DC loss reduced by ~ 21.70, 5.23, and 3.84%, respectively compared to the jacket cooling. On the contrary, AC loss depends on the electrical resistance of the winding and magnetic flux density (see Eq. (7)). Higher electrical conductivity, and magnetic flux density along with compact winding configuration of DWHX results in significantly higher AC loss compared to other configurations. At a current density of 17.37 A/mm^2 and in case of DWHX cooling, AC loss increased by ~ 48.28% compared to jacket cooling. Furthermore, slightly lower electrical resistance as a consequence of lower temperature in circular and rectangular stator channel cooled machines results in marginally higher AC loss despite the reduced flux density. However, at any particular current density, DC loss is significantly higher than the AC loss, and this trend amplifies with current density. Therefore, total winding loss follows the DC loss trend as shown in Fig. 12 (c). For DWHX cooling, total winding loss reduced by ~ 12.72% compared to the jacket cooling.

Fig. 13 shows the stator loss variation with electrical loading for all cooling configurations. Stator loss is composed of hysteresis and eddy current losses, and both components depend on magnetic flux density. Same stator configuration in jacket cooling and DWHX configurations results in equal stator eddy current, and comparable flux density distributions, leading to similar stator loss. On the contrary, rectangular and circular stator channel configurations reduce the eddy current, and reduced d and q-axis flux linkage, collectively resulting in reduced stator loss compared to other two configurations. For circular and rectangular channel configurations and at a current density of 17.37 A/mm^2, stator loss reduced by ~ 15.92, and 28.50% compared to the jacket cooling.

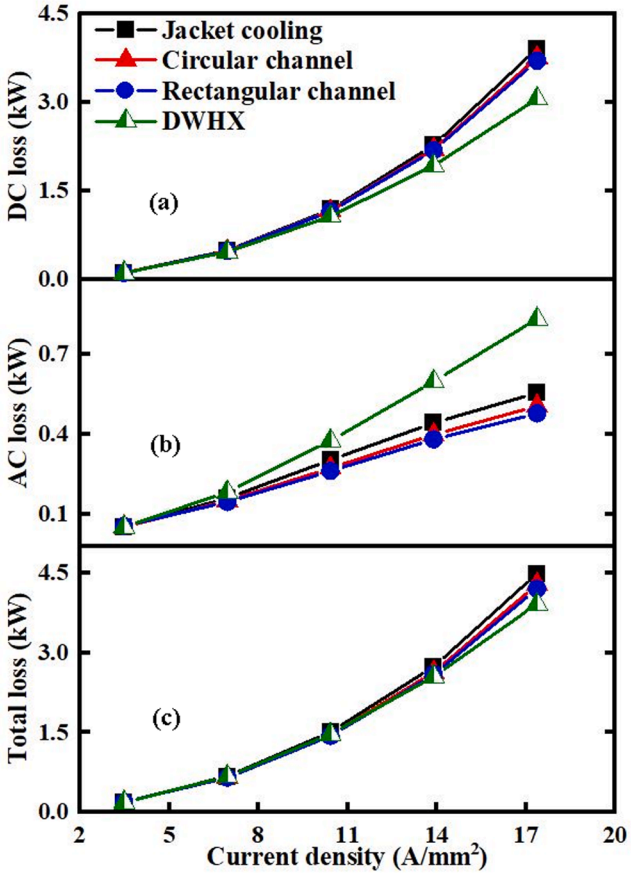

Fig. 12. DC loss, AC loss, and total winding loss as a function of current density for all cooling configurations while maintaining a constant speed, current density, phase advance, and convective heat transfer coefficient of 4,500 rpm, 17.37 A/mm^2, 45 EDeg, and 5,000 W/m^2.K, respectively.

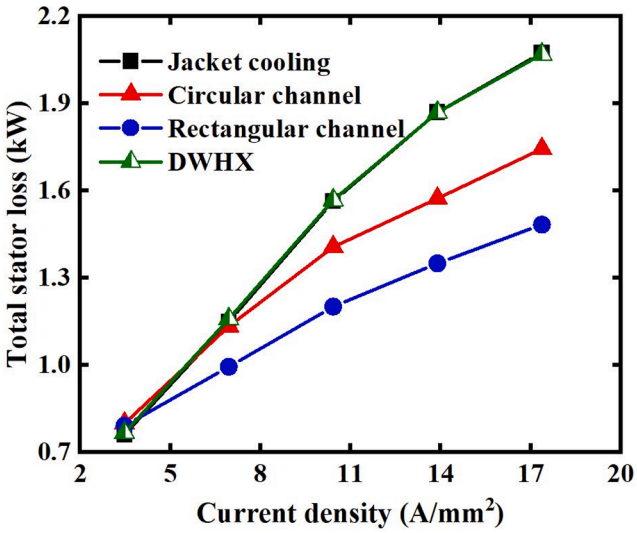

Fig. 13. Stator loss as a function of current density for all cooling configurations while maintaining a constant speed, current density, phase advance, and convective heat transfer coefficient of 4,500 rpm, 17.37 A/mm^2, 45 EDeg, and 5,000 W/m^2.K, respectively. Note that the stator loss for DWHX and jacket cooling are overlapping.

7.4. Overall Performance

Fig. 14 illustrates the efficiency as a function current density for all proposed cooling configurations. For all configurations, motor efficiency

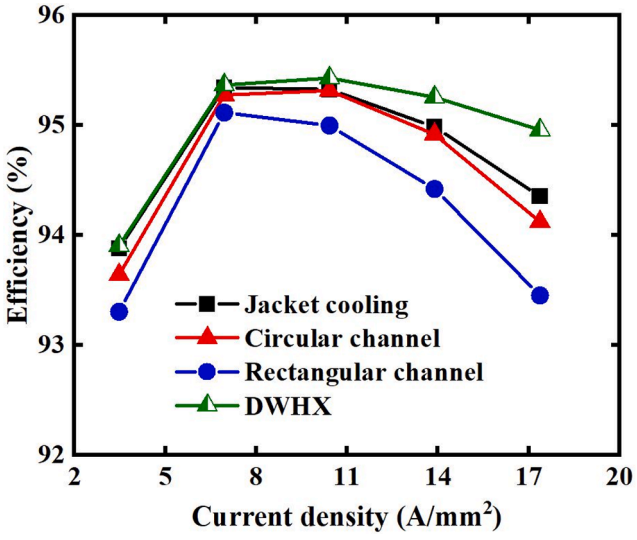

Fig. 14. Efficiency as a function of current density for all cooling configurations while maintaining a constant speed, current density, phase advance, and convective heat transfer coefficient of 4,500 rpm, 17.37 A/mm^2, 45 EDeg, and 5,000 W/m^2.K, respectively.

reaches a peak value at a current density of 6.95 A/mm^2. After this threshold, efficiency starts to reduce regardless of the cooling configuration. This behavior can be explained from the torque and loss variation with electrical loading. Shaft torque increases almost linearly with the current density (see Fig. 9), whereas winding loss increases quadratically with the current density (see Fig. 12 (a)). Additionally, significantly lower shaft torque generated by rectangular and circular channel cooled machines (see Fig. 9) along with higher winding loss results (see Fig. 12 (a) and (c)) in lower efficiency, as shown in the Fig. 14. For example, in case of circular and rectangular stator channel configurations and at a current density of 17.37 A/mm^2, efficiency reduced by ~ 0.88, and 1.59% compared to the DWHX cooling. On the contrary, under the same electrical loading, motor efficiency can be increased by ~ 0.64% utilizing DWHX cooling compared to the jacket cooling.

8. Conclusion

This paper compares the electro-magnetic and thermal performance of four different cooling techniques, namely jacket cooling, stator integrated circular cross-section and rectangular cross-section channels, and direct winding heat exchanger (DWHX) cooling. The effectiveness of all cooling configurations has been investigated numerically by implementing these in a 125 kW BMW i3 motor. A two-way coupled algorithm has been utilized for the electro-magnetic and thermal simulations. The magnetic flux distribution and torque were similar for the jacket cooling and DWHX. On the other hand, the rectangular and circular cooling channels hinder the flux flow path in the stator back iron and results in poor electro-magnetic performance. Temperature distributions for all cases showed that the peak temperature occurs in the windings, and the lowest temperature occurs toward the outside of the stator, except for the DWHX, for which the minimum temperature occurs in the slot winding. Of the techniques studied, the DWHX provided the lowest winding temperatures followed by rectangular and circular channels, particularly because of its higher convection surface area and reduced thermal resistances. By employing DWHX, rectangular and circular channels, motor temperature can be reduced by ~ 88–102 °C, ~19–29 °C, and ~ 14–20 °C, respectively, compared to the jacket cooling. In general, the DWHX technique yields better thermal performance, lower electro-magnetic losses, and hence, better overall performance, i.e., higher efficiency than stator channel cooled techniques. It can be concluded that the enhanced performance of the DWHX demonstrates its capabilities as a state-of-the-art approach in terms of overall electro-magnetic performance and thermal management.

Declaration of Competing Interest

The authors declare that they have no known competing financial interests or personal relationships that could have appeared to influence the work reported in this paper.

Acknowledgements

The information, data, or work presented herein was funded in part by the Advanced Research Projects Agency-Energy (ARPA-E), U.S. Department of Energy, under Award Number DE-AR0001023 in the OPEN 2018 program monitored by Dr. Michael Ohadi. The views and opinions of authors expressed herein do not necessarily state or reflect those of the United States Government or any agency thereof. The authors would like to thank Md. Shariful Islam at North Carolina State University for his valuable suggestion.

References

[1] A. Singh, Electric Vehicle Market by Type, Apr 2020. [Online]. Available: https://www.alliedmarketresearch.com/electric-vehicle-market.
[2] J. Jang, H.-C. Chu, W.-M. Yan, M. Tsai, P.-Y. Wang, Numerical study on electromagnetics and thermal cooling of a switched reluctance motor, Case Studies in Thermal Engineering 6 (2015) 16–17.
[3] J. Pyrhonen, P. Lindh, M. Polikarpova, E. Kurvinen, V. Naumanen, Heat-transfer improvements in an axial-flux permanent-magnet synchronous machine, Applied Thermal Engineering 76 (2015) 245–251.
[4] M.H. Park, S.C. Kim, Thermal characteristics and effects of oil spray cooling on in-wheel motors in electric vehicles, Applied Thermal Engineering 152 (2019) 582–593.
[5] C. Kim, K.-S. Lee, S.-J. Yook, Effect of air-gap fans on cooling of windings in a large-capacity, high-speed induction motor, Applied Thermal Engineering 100 (2016) 658–667.
[6] S.A. Semidey, J.R. Mayor, Experimentation of an Electric Machine Technology, IEEE Transactions on Industrial Electronics 61 (10) (2014) 5771–5778.
[7] Y. Sun, S. Zhang, G. Chen, Y. Tang, F. Liang, Experimental and numerical investigation on a novel heat pipe based cooling strategy for permanent magnet synchronous motors, Applied Thermal Engineering 170 (2020), 114970.
[8] H. Li, "Cooling of a permanent magnet electric motor with centirfugal impeller," Int, Journal of Heat and Mass Transfer 53 (2020) 797–810.
[9] Y. Zhang, J. Ruan, T. Huang, X. Yang, Calculation of Temperature Rise in Air-cooled Induction Motors Through 3-D Coupled Electromagnetic Fluid-Dynamical and Thermal Finite-Element Analysis, IEEE Transactions on Magnetics 48 (2) (2012) 1047–1050.
[10] M. Satrustegui, M. Martinez-Iturralde, J.C. Ramos, P. Gonzalez, G. Astarbe, I. Elosgui, Design criteria for water cooled systems of induction machines, Applied Thermal Engineering 114 (2017) 1018–1028.
[11] S. Lundmark, A. Acquaviva, Coupled 3-D Thermal and Electromagnetic Modelling of a Liquid-cooled Transverse Flux Traction Motor. in 2018 XIII International Conference on Electrical Machines (ICEM), 2018.
[12] A.J. Mitcham, A.G. Razzell, Stator Core, Patent 7288870B2 (October 2007) 30.
[13] H. Stiesdal, Generator with a stator comprising cooling channels and method for cooling a laminated stator of a generator. Spain Patent 2415661T3, 26 July 2013.
[14] S. Munro, Tearing Down Tesla Segment 8: Comparing the Cooling Strategy / Housings of Motors for Tesla Model 3 vs BMW i3, Lean Design, 10 March 2020. [Online]. Available: https://leandesign.com/tearing-down-tesla-segment-8-comparing-the-cooling-strategy-housings-of-motors-for-tesla-model-3-vs-bmw-i3/. [Accessed 11 May 2020].
[15] A. Kumar, S. Marwaha, A. Marwaha, N. Kalsi, Magnetic field analysis of induction motor for optimal cooling duct design, Simulation Modeling Practice and Theory 18 (2) (2010) 157–164.
[16] K.-H. Lee, H.-R. Cha, Y.-B. Kim, Development of an interior permanent magnet motor through rotor cooling for electric vehicles, Applied Thermal Engineering 95 (2016) 348–356.
[17] J.-X. Wang, Y.-Z. Li, S.-N. Wang, H.-S. Zhang, X. Ning, W. Guo, Experimental investigation of the thermal control effects of phase change material based packaging strategy for on-board permanent magnet synchronous motors, Energy Conversion and Management 123 (2016) 232–242.
[18] S. Wang, Y. Li, Y.-Z. Li, J. Wang, X. Xiao, W. Guo, Transient cooling effect analyses for a permanent-magnet synchronous motor with phase-change-material packaging, Applied Thermal Engineering 109 (2016) 251–260.
[19] J.-X. Wang, W. Guo, K. Xiong, S.-N. Wang, Review of aerospace-oriented spray cooling technology, Progress in Aerospace Sciences 116 (2020).
[20] K. Xiong, Y. Li, Y.-Z. Li, J.-X. Wang, Power loss and efficiency analysis of an onboard three-level brushless synchronous generator, International Journal of Electronics (2020).
[21] J.-X. Wang, Y.-Z. Li, X.-K. Yu, G.-C. Li, X.-Y. Ji, Investigation of heat transfer mechanism of low environmental pressure large-space spray cooling for near-space flight systems, International Journal of Heat and Mass Transfer 119 (2018) 496–507.
[22] J.-X. Wang, Y.-Z. Li, J.-X. Li, C. Li, Y. Zhang, X.-W. Ning, A gas-atomized spray cooling system integrated with an ejector loop: Ejector modeling and thermal performance analysis, Energy Conversion and Management 180 (2019) 106–118.
[23] Y. Peles, A. Kosar, C. Mishra, C.-J. Kuo, B. Schneider, Forced convective heat transfer across a pin fin micro heat sink, International Journal of Heat and Mass Transfer 48 (17) (2005) 3615–3627.
[24] A. Acquaviva, S. Skoog, T. Thiringer, Design and Verification of In-slot Oil-Cooled Tooth Coil Winding PM Machine for Traction Application, in: IEEE Transactions on Industrial Electronics.
[25] I. Petrov, P. Lindh, M. Niemelä, E. Scherman, O. Wallmark, J. Pyrhönen, Investigation of a Direct Liquid Cooling System in a Permanent Magnet Synchronous Machine, IEEE Transactions on Energy Conversion 35 (2) (June 2020) 808–817.
[26] K. Xiong, Y. Li, Y.-Z. Li, Ji-Xiang, Y. Mao, Numerical Investigation on the Thermal Performance of Nanofluid-Based Cooling System for Synchronous Generators, Entropy 21 (420) (2019).
[27] B. Silwal, A.H. Mohamed, J. Nonneman, M.D. Paepe, P. Sergeant, Assessment of Different Cooling Techniques for Reduced Mechanical Stress in the Windings of Electrical Machines, Energies 12 (1967) (2019) 1–18.
[28] B. Ozpineci, Oak Ridge National Laboratory Annual Progress Report for the Electric Drive Technologies Program, U.S. Department of Energy, Washington, D.C., 2016.
[29] [Online] Available: https://www.arnoldmagnetics.com/wpcontent/uploads/2019/06/Arnold-Neo-Catalog.pdf.
[30] W. Sixel, M. Liu, G. Nellis, B. Sarlioglu, Cooling of Windings in Electric Machines via 3D Printed Heat Exchanger, 2018 IEEE Energy Conversion Congress and Exposition (ECCE), Portland, OR, 2018.

[31] [Online]. Available: https://www.engineeringtoolbox.com/permeability-d_1923.html.
[32] Hu Jianhui, Zou Jibin and Liang Weiyan, Finite element calculation of the saturation DQ-axes inductance for a direct drive PM synchronous motor considering cross-magnetization, The Fifth International Conference on Power Electronics and Drive Systems, 2003. PEDS 2003, Singapore, 2003, pp. 677-681 Vol.1.
[33] [Online]. Available: https://www.motor-design.com/publications/MotorCAD Manual.pdf.
[34] Y.S. Chen, Z.Q. Zhu, D. Howe, Calculation of d- and q-axis inductances of PM brushless ac machines accounting for skew, IEEE Transactions on Magnetics 41 (10) (Oct. 2005) 3940–3942.
[35] S.M. Ghiaasiaan, Convective Heat and Mass Transfer, Boca Raton, CRC Press, FL, 2018.
[36] M.S. Islam, I. Husain, A. Ahmed, A. Sathyan, Asymmetric Bar Winding for High-Speed Traction Electric Machines, IEEE Transactions on Transportation Electrification 6 (1) (March 2020) 3–15.
[37] W.D. Morris, J.L. Woods, Heat Transfer in the Entrance Region of Tubes that Rotate about a Parallel Axis, Journal of Mechanical Engineering Science 20 (6) (1978) 319–325.
[38] Le Feuvre, R. F., Heat Transfer in Rotor Cooling Ducts, Proceedings of the Institution of Mechanical Engineers, Conference Proceedings, 182(8), 232–240, 1967.
[39] L. Cuiping, P. Yulong, N. Ronggang and C. Shukang, Analysis of 3D static temperature field of water cooling induction motor in mini electric vehicle, in 2011 International Conference on Electrical Machines and Systems, 2011.
[40] Y. Shi, J. B. Wang and B. Wang, Transient 3D Lumped Parameter and 3D FE Thermal Models of a PMASynRM under Fault Conditions with Asymmetric Temperature Distribution, in: IEEE Transactions on Industrial Electronics.
[41] N. Simpson, R. Wrobel and P. H. Mellor, Estimation of Equivalent Thermal Parameters of Impregnated Electrical Windings, in: IEEE Transactions on Industry Applications, vol. 49, no. 6, pp. 2505-2515, Nov.-Dec. 2013.
[42] A. Tikadar, N. Kumar, Y. Joshi, S. Kumar, Coupled Electro-Thermal Analysis of Permanent Magnet Synchronous Motor for Electric Vehicles, IEEE ITherm Conference (2019).